ORIGINAL ARTICLE

Improving GNSS PPP-RTK through global forecast system zenith wet delay augmentation

Rui Gao[1,2,3] · Zhizhao Liu[3] · Robert Odolinski[4] · Baocheng Zhang[1]

Abstract

The precise point positioning real-time kinematic (PPP-RTK) is a high-precision global navigation satellite system (GNSS) positioning technique that combines the advantages of wide-area coverage in precise point positioning (PPP) and of rapid convergence in real-time kinematic (RTK). However, the PPP-RTK convergence is still limited by the precision of slant ionospheric delays and tropospheric zenith wet delay (ZWD), which affects the PPP-RTK network parameters estimation and user positioning performance. The present study aims to construct a PPP-RTK model augmented with a priori ZWD values derived from the global forecast system (GFS) product (a global numerical weather prediction (NWP) model) to improve the PPP-RTK performance. This study gives a priori ZWD values and conversion based on the GFS products, and the full-rank GFS-augmented undifferenced and uncombined (UDUC) PPP-RTK network model is derived. To verify the performance of GFS-augmented UDUC PPP-RTK, a comprehensive evaluation using 10-day GNSS observation data from three different GNSS station networks in the United States (US), Australia, and Europe is conducted. The results show that with the GFS ZWD a priori information, PPP-RTK performance significantly improves at the initial filtering stage, but this advantage gradually decays over time. Based on 10-day positioning results for all user stations, the GFS ZWD-augmented PPP-RTK approach reduces the average convergence time by 46% from 10.0 to 5.4 min, the three-dimensional root-mean-square (3D-RMS) error by 5.7% from 3.5 to 3.3 cm, and the time to first fix (TTFF) value by 35.8% from 6.7 to 4.3 min, all when compared to the traditional PPP-RTK without GFS ZWD constraints.

Keywords GPS · PPP-RTK · Tropospheric delay · Numerical weather prediction (NWP) · Positioning performance

✉ Zhizhao Liu
   lsszzliu@polyu.edu.hk

✉ Baocheng Zhang
   b.zhang@whigg.ac.cn

[1] Innovation Academy for Precision Measurement Science and Technology, Chinese Academy of Sciences, Wuhan, China

[2] College of Earth and Planetary Sciences, University of Chinese Academy of Sciences, Beijing, China

[3] Department of Land Surveying and Geo-Informatics, Hong Kong Polytechnic University, Hung Hum, Kowloon, Hong Kong

[4] School of Surveying, University of Otago, Dunedin, New Zealand

Introduction

As an important error in radio-based geodetic surveying techniques, the tropospheric delay significantly impacts GNSS signals and can reach 2–3 m in the zenith direction (Yu et al. 2018). The influence of the tropospheric delay on GNSS signals severely limits the performance of GNSS positioning (Wilgan et al. 2017). Therefore, modeling tropospheric delay has always been an important topic in the field of GNSS and a vexing issue in high-accuracy GNSS technologies.

PPP-RTK, as a high-precision GNSS positioning method, has been widely studied and applied in the GNSS field (Teunissen and Khodabandeh 2015). In PPP-RTK, GNSS reference station network generates real-time correction information, which are broadcast to the user stations in a state-space representation (Zhang et al. 2019). This information allows user stations to achieve centimeter-level positioning in real-time (Zhang et al. 2022).

During the PPP-RTK solution process, the tropospheric delay is usually divided into two parts: tropospheric zenith hydrostatic delay (ZHD) and ZWD (Hou and Zhang 2023). The ZHD accounts for about 90% of the tropospheric zenith total delay and can be accurately calculated using mature tropospheric models (Leandro et al. 2008). In contrast, the ZWD is caused by complex and various factors, and it is difficult to model. PPP-RTK technology involves both the user model that requires positioning and the network model that provides for the positioning products. These two models normally use different approaches to solve the ZWD. For the user model, it can rely on the tropospheric ZWD correction information provided by the reference station network to construct an interpolation model (Hou and Zhang 2023), fitting model (Cui et al. 2022), or grid model (Yin et al. 2022) to obtain the ZWD at user location. Then, the user employs this information to correct or constrain the ZWD parameter in the PPP-RTK user model. For the PPP-RTK network model, it is generally challenging to mitigate the impact of ZWD by differencing or using the spatial correlation of atmospheric conditions when the interstation distance exceeds 20 km (Deng et al. 2014; Gurturk and Soycan 2021). Therefore, it is necessary to carefully consider the method of processing tropospheric wet delay in the PPP-RTK network model.

In the processing of tropospheric wet delay in GNSS algorithms, it is common to estimate the ZWD parameter by combining it with the tropospheric mapping function, which is derived from tropospheric models and is dependent on the elevation angle of the satellite (Böhm et al. 2015). However, this method increases the number of unknown parameters and reduces the model strength. Some studies have attempted to utilize external devices to correct or constrain the tropospheric wet delay (Wang and Liu 2019). For instance, Wang and Liu (2019) enhanced PPP accuracy by using water vapor radiometers (WVR), achieving a 3% vertical accuracy improvement for static PPP and 10% for dynamic PPP, as well as a 30–50% reduction in convergence time of the positioning errors. Nonetheless, the high cost of WVR hinders its wide application in the GNSS community. Recently, the significant improvements in the accuracy and spatial resolution of NWP models have made it possible to model the troposphere more precisely, providing new solutions for processing tropospheric wet delay in GNSS (Powers et al. 2017; Wilgan et al. 2017). Lu et al. (2017) used ZWD values from the GFS, a global NWP model provided by the National Centers for Environmental Prediction (NCEP), which reduced the convergence time of PPP by 60% and improved the positioning accuracy by 40%. These studies demonstrate the effectiveness of NWP products and their contribution to improving the GNSS positioning performance.

The previous studies showed that NWP has successfully been employed in the GNSS PPP technology. PPP-RTK, another advanced GNSS positioning technique, is also confronted by the challenge of processing tropospheric wet delay with high precision. However, the research on integrating NWP ZWD information with GNSS technology is not extensive (Theodoro et al. 2022), and no studies have reported the performance of NWP ZWD-augmented PPP-RTK.

In this contribution, we aim to develop a UDUC PPP-RTK model augmented with GFS ZWD and comprehensively evaluate the performance improvement of the PPP-RTK model using GFS products (Lu et al. 2017). In this paper, we first introduce the method of obtaining water vapor data in GFS products and the method of converting water vapor data and GNSS reference station ZWD parameters. Then, we add the ZWD pseudo-observation information obtained from GFS to constrain the estimated ZWD parameters in the PPP-RTK network model. Finally, we eliminate all types of rank deficiency in the observation equations by S-basis theory to obtain the full-rank GFS ZWD-augmented PPP-RTK network model. To validate the performance of the GFS ZWD-augmented PPP-RTK in different regions of the world, three GNSS networks from the National Geodetic Survey (NGS) of the US, Geoscience Australia (GA), and European Reference Permanent GNSS Network (EPN), respectively, are selected to conduct kinematic PPP-RTK solutions. Ten days (day of year (DOY) 60–69 in 2022) of GNSS observation data are analyzed. By comparing the results of traditional PPP-RTK without GFS ZWD augmentation, we validate the performance improvement of the PPP-RTK model in terms of positioning error convergence time, positioning accuracy, and ambiguity resolution.

Method

A priori ZWD acquisition from GFS product

GFS provides various global atmospheric prediction products and distributes them on the geographic grid with a resolution of $0.25° \times 0.25°$ (Han and Pan 2011). The temporal resolution of GFS products provided by the NCEP is 3 h. In this study, precipitable water vapor (PWV), surface geopotential height, and surface temperature datasets are extracted from GFS products for a priori ZWD acquisition of GNSS stations. To obtain PWV data for each GNSS station, we first determine the GFS geographical grid in which the GNSS station is located and select PWV and surface geopotential height datasets at the four grid references of the geographical grid. Then, the Kouba model (Kouba 2008) is

used to convert the PWV data at the four grid references to the PWV value at the GNSS station:

$$\mathrm{PWV}_{h_s} = \mathrm{PWV}_{h_0} \cdot \exp\left(\frac{h_0 - h_s}{2000}\right) \tag{1}$$

where h_0 and h_s denote geopotential height values of surface and GNSS station, respectively; PWV_{h_0} is PWV value at the surface geopotential height provided by GFS product; and PWV_{h_s} is PWV value at the height of GNSS station. At the four grid references, their PWV values at surface geopotential heights are converted to the height same as that of the GNSS station using the Kouba model. Thus, the PWV datasets at the four grid references are on the same plane as the GNSS station. Then, the a priori ZWD at these references can be derived from PWV using the conversion factor Π (Bevis et al. 1994):

$$\mathrm{ZWD}_{x_i,y_i} = \mathrm{PWV}_{x_i,y_i}/\Pi \tag{2}$$

where ZWD (PWV)$_{x_i,y_j}$ denotes the ZWD (PWV) value at the plane coordinates (x_i, y_j). Conversion factor Π can be calculated using the following:

$$\Pi = \frac{10^6}{\rho R_v \left(\frac{k_3}{T_m} + k_2'\right)} \tag{3}$$

where ρ is the density of liquid water; R_v is the gas constant of water vapor; k_2' and k_3 are physical constants given in Bevis et al. (1994); and T_m is the weighted mean temperature of atmosphere calculated from the Bevis model (Bevis model: $T_m \approx 0.72T_p + 70.2$, T_p is the temperature at the solution position). We can use the surface temperature datasets at the geographic grid references provided by GFS to calculate the conversion factor at geographic grid references. Then, the a priori ZWD values at the four grid references are obtained. Finally, the bilinear interpolation method can be used to obtain the a priori GFS ZWD value at the position of the GNSS station (Accadia et al. 2003):

$$\begin{cases} \mathrm{ZWD}_s \approx \frac{y_2 - y_s}{y_2 - y_1}\mathrm{ZWD}_{x_s,y_1} + \frac{y_s - y_1}{y_2 - y_1}\mathrm{ZWD}_{x_s,y_2} \\ \mathrm{ZWD}_{x_s,y_1} \approx \frac{x_2 - x_s}{x_2 - x_1}\mathrm{ZWD}_{x_1,y_1} + \frac{x_s - x_1}{x_2 - x_1}\mathrm{ZWD}_{x_2,y_1} \\ \mathrm{ZWD}_{x_s,y_2} \approx \frac{x_2 - x_s}{x_2 - x_1}\mathrm{ZWD}_{x_1,y_2} + \frac{x_s - x_1}{x_2 - x_1}\mathrm{ZWD}_{x_2,y_2} \end{cases} \tag{4}$$

where ZWD_s denotes the ZWD value at the GNSS station; $x_{1,2}$ and $y_{1,2}$ are plane coordinates of the four grid references; and x_s and y_s are plane coordinates of GNSS station.

GNSS observation equations

The linearized equations for GNSS code and phase observables are given below:

$$E\left[p_{r,j}^s\right] = g_r^s \Delta x_r + m_r^s \tau_r + \mathrm{d}t_r - \mathrm{d}t^s + \mu_j l_r^s + d_{r,j} - d_j^s$$

$$E\left[\phi_{r,j}^s\right] = g_r^s \Delta x_r + m_r^s \tau_r + \mathrm{d}t_r - \mathrm{d}t^s - \mu_j l_r^s + \delta_{r,j} - \delta_j^s + \lambda_j z_{r,j}^s \tag{5}$$

where r, s, and j denote GNSS receiver, satellite, and frequency indices, respectively; $E[\cdot]$ denotes the expectation operator; and $p_{r,j}^s(\phi_{r,j}^s)$ is the observed-minus-computed code (phase) observation, measured by receiver r from satellite s on frequency j. The estimated parameters and their coefficients include: Δx_r denotes the receiver position increment, and the receiver-to-satellite unit direction vector g_r^s is its coefficient; τ_r is the tropospheric ZWD for receiver r; mapping function m_r^s is its coefficient; $\mathrm{d}t_r$ is the receiver clock error; $\mathrm{d}t^s$ is the satellite clock error; $d_{r,j}(\delta_{r,j})$ is the receiver code (phase) bias; and $d_j^s(\delta_j^s)$ is the satellite code (phase) bias. l_r^s is the ionospheric delay, and scalar $\mu_j = f_1^2/f_j^2$ is its coefficient (f_j being the frequency); and $z_{r,j}^s$ is the ambiguity with the wavelength λ_j as its coefficient. Only dual-frequency data are used in this paper, thus $j = 1, 2$.

GFS-augmented UDUC PPP-RTK network model

In order to facilitate parameter combination, the receiver and satellite code biases are transformed into the following form (Teunissen and Khodabandeh 2015):

$$d_{r,j} = d_{r,\mathrm{IF}} + \mu_j d_{r,\mathrm{GF}}$$

$$d_j^s = d_{\mathrm{IF}}^s + \mu_j d_{\mathrm{GF}}^s \tag{6}$$

where $d_{r,\mathrm{IF}}$ and d_{IF}^s denote ionosphere-free (IF) combination code biases for receiver and satellite, respectively; $d_{r,\mathrm{GF}}$ and d_{GF}^s are geometry-free (GF) combination code biases for receiver and satellite, respectively.

In undifferenced and uncombined PPP-RTK network processing, the ionosphere-weighted method has been proven useful for enhancing network product performance, which can improve user positioning, positioning convergence time, and ambiguity fixing (Odolinski et al. 2015). So, we add a constraint for single-difference ionosphere parameter using the ionospheric pseudo-observation $E\left[l_{1r}^s\right] = l_r^s - l_1^s$. Index 1 denotes the datum receiver or satellite, and any station or satellite can be selected as the datum to achieve reparameterization. In addition, the a priori ZWD datasets provided by GFS product can be used to constrain the ZWD parameter to be estimated in the GNSS observation equations to further enhance the model strength. This can be achieved by adding tropospheric pseudo-observations $E[\tau_r] = \tau_r$. Furthermore, the parameter of receiver position increment is not shown in the network model because we assume that the positions of all network reference stations are known. Then, we can get:

$$E\left[p_{r,j}^s\right] = m_r^s \tau_r + \mathrm{d}t_r - \mathrm{d}t^s + \mu_j l_r^s + d_{r,\mathrm{IF}} + \mu_j d_{r,\mathrm{GF}} - d_{\mathrm{IF}}^s - \mu_j d_{\mathrm{GF}}^s$$

$$E\left[\phi_{r,j}^s\right] = m_r^s \tau_r + \mathrm{d}t_r - \mathrm{d}t^s - \mu_j l_r^s + \delta_{r,j} - \delta_j^s + \lambda_j z_{r,j}^s$$

$$E\left[l_{1r}^s\right] = l_r^s - l_1^s$$

$$E\left[\tau_r\right] = \tau_r$$

$$\tag{7}$$

where $E\left[l_{1r}^s\right] = 0$, and the constraint strength is controlled by a stochastic model which is dependent on the separation of reference stations. $E\left[\tau_r\right] = \mathrm{ZWD}_r$, and the constraint is dependent on the accuracy of the GFS ZWD product. GFS 3-h ZWD forecast products are used in this study. The accuracy of the product relies on factors such as atmospheric humidity and weather conditions (Lasota et al. 2020). The standard deviation of GFS ZWD short-range forecast product is approximately 2 cm (Lu et al. 2017).

The observation equations in (7) are rank deficient. The rank deficiencies can be eliminated by identifying the null space of the design matrix and choosing a minimum set of constraints (S-basis) (Teunissen 1985). It is worth noting that this model uses broadcast ephemeris and that satellite clock errors are estimated by the network model. All parameters estimated by the network are self-consistent. In a regional reference station network, due to the introduction of estimable satellite clock error in the network model, a rank deficiency almost exists between the columns of τ_r and $\mathrm{d}t^s$ (Kleijer 2004). This is because in a regional reference station network, the mapping functions of the reference stations are nearly the same ($m_1^s \approx m_2^s \approx ... \approx m_n^s$, n denotes the number of the reference stations in the regional network), and it will cause the troposphere τ_r and satellite clock $\mathrm{d}t^s$ to be highly correlated. The tropospheric ZWD of the pivot receiver τ_1 can be used as a datum to eliminate this nearly rank deficiency. Thus, the ZWD parameter we estimate is in single-differenced form. The estimable full-rank model can be derived after identifying and solving all the rank deficiencies (Gao et al. 2023). Finally, the full-rank GFS-augmented UDUC PPP-RTK network model based on a dual-frequency dataset is given below:

$$E\left[p_{r,j}^s\right] = m_r^s \tilde{\tau}_r + \mathrm{d}\tilde{t}_r - \mathrm{d}\tilde{t}^s + \mu_j \tilde{l}_r^s + \mu_j \tilde{d}_{r,\mathrm{GF}}$$

$$E\left[\phi_{r,j}^s\right] = m_r^s \tilde{\tau}_r + \mathrm{d}\tilde{t}_r - \mathrm{d}\tilde{t}^s - \mu_j \tilde{l}_r^s + \tilde{\delta}_{r,j} - \tilde{\delta}_j^s + \lambda_j \tilde{z}_{r,j}^s$$

$$E\left[l_{1r}^s\right] = \tilde{l}_r^s - \tilde{l}_1^s$$

$$E\left[\tau_{1r}\right] = \tilde{\tau}_r$$

$$\tag{8}$$

where $E\left[\tau_{1r}\right] = \mathrm{ZWD}_{r,r\neq1} - \mathrm{ZWD}_1$ is provided by the GFS product. It is used to constrain the single-difference ZWD parameter to in the GFS ZWD-augmented PPP-RTK. The estimable unknowns in (8) are denoted with a 'tilde.' It is worth noting that the GF receiver code biases (RCB) $\tilde{d}_{r,\mathrm{GF}}$ are estimable, due to the introduction of ionospheric pseudo-observations. It also ensures that all estimable ionospheric delay parameters absorb the same RCB from the datum reference station, which the user's RCB estimates will eventually absorb. All the estimable unknown parameters and their estimable forms are shown in Table 1. Note that the UNB3m tropospheric model is used to calculate the mapping function of tropospheric ZWD and to correct the hydrostatic component of the tropospheric error (Leandro et al. 2008). In both the network and user models, the mapping function is used to construct the design matrix, while the hydrostatic component of the tropospheric error is directly corrected in the observed-minus-computed observation.

For clarity, the aforementioned full-rank function model (8) is presented in a single-epoch form. In this study, the Kalman filter is employed. In the parameter process noise settings in the Kalman filter of the PPP-RTK network model, we estimate satellite/receiver clock and ionospheric delays as white noise, satellite/receiver bias as time-constant, tropospheric wet delays as random-walk noise, and ambiguities as float constants for each arc.

The stochastic model of the GFS ZWD-augmented PPP-RTK network model is given as follows:

$$Q = \mathrm{blkdiag}\left(Q_{\mathrm{yy}}, Q_I, Q_\tau\right) \tag{9}$$

Table 1 Estimable parameters of the GFS-augmented UDUC PPP-RTK network model

Parameter	Formulation	Description
$\tilde{\tau}_r$	$\tau_r - \tau_1$	Single-differenced (SD) ZWD
$\mathrm{d}\tilde{t}_r$	$\left(\mathrm{d}t_r + d_{r,\mathrm{IF}}\right) - \left(\mathrm{d}t_1 + d_{1,\mathrm{IF}}\right)$	Estimable receiver clock error
$\mathrm{d}\tilde{t}^s$	$\left(\mathrm{d}t^s + d_{\mathrm{IF}}^s\right) - \left(\mathrm{d}t_1 + d_{1,\mathrm{IF}}\right) - m_1^s \tau_1$	Estimable satellite clock error
$\tilde{l}_r^s$	$l_r^s - \left(d_{\mathrm{GF}}^s - d_{1,\mathrm{GF}}\right)$	Estimable slant ionospheric delay
$\tilde{d}_{r,GF}$	$d_{r,\mathrm{GF}} - d_{1,\mathrm{GF}}$	SD GF receiver code biases
$\tilde{\delta}_{r,j}$	$\left(\delta_{r,j} - d_{r,\mathrm{IF}}\right) - \left(\delta_{1,j} - d_{1,\mathrm{IF}}\right) + \lambda_j\left(z_{r,j}^1 - z_{1,j}^1\right)$	Estimable receiver phase biases
$\tilde{\delta}_j^s$	$\left(\delta_j^s - d_{\mathrm{IF}}^s\right) - \left(\delta_{1,j} - d_{1,\mathrm{IF}}\right) + \mu_j\left(d_{\mathrm{GF}}^s - d_{1,\mathrm{GF}}\right) - \lambda_j z_{1,j}^s$	Estimable satellite phase biases
$\tilde{z}_{r,j}^s$	$(z_{r,j}^s - z_{1,j}^s) - (z_{r,j}^1 - z_{1,j}^1)$	Double-differenced ambiguity

where Q_{yy}, Q_I, and Q_τ are variance–covariance of GNSS observations, ionospheric, and tropospheric pseudo-observations, respectively; and 'blkdiag' denotes a block diagonal matrix. The stochastic model for the GNSS code/phase observations Q_{yy} is based on an elevation-dependent weighting scheme. The variance–covariance matrix for the UDUC code/phase observations is given as follows:

$$Q_{yy} = \text{blkdiag}\left(C_p, C_\phi\right) \otimes Q_m \otimes E_n \qquad (10)$$

where $C_p = \text{diag}\left(\sigma_{p,j=1}^2, \sigma_{p,j=2}^2\right)$ and $C_\phi = \text{diag}\left(\sigma_{\phi,j=1}^2, \sigma_{\phi,j=2}^2\right)$ are the variance–covariance matrices for the a priori GNSS code and phase observations in the zenith direction, respectively, and 'diag' denotes a diagonal matrix. The a priori standard deviation (STD) in the zenith direction for the GNSS code and phase observations is set as 0.3 m and 0.003 m, respectively. $Q_m = \text{diag}\left(\left(\sin^2 e^1\right)^{-1}, \cdots, \left(\sin^2 e^s\right)^{-1}\right)$ is the elevation-dependent weighting function with the satellite elevation e (Eueler and Goad 1991); and $\otimes$ is the Kronecker product (Teunissen et al. 2014). E_n is an identity matrix with a size same as the number of reference stations n.

The stochastic model for the ionospheric pseudo-observations is $Q_I = \text{diag}\left(\sigma_{2,I}^2, ..., \sigma_{n,I}^2\right) \otimes Q_m$ which depends on the ionosphere delay uncertainty and the distance between the reference station and the datum reference station $L_{r\neq1}$ (Li et al. 2022). In this study, for these regional PPP-RTK networks, the slant ionospheric delay STD is modeled as an empirical function $\sigma_{r\neq1,I} = 1.4 \times 0.001 \cdot L_{r\neq1}$, which is 1.4 mm/km (Odolinski and Teunissen 2017; Schaffrin and Bock 1988).

The stochastic model of the tropospheric pseudo-observations depends on the accuracy of GFS PWV product, which is an empirical value. The variance–covariance matrix of the tropospheric pseudo-observations is given as follows:

$$Q_\tau = \text{SD} \cdot \left(\sigma_{ZWD}^2 \cdot E_n\right) \cdot \text{SD}^T \qquad (11)$$

where SD is the single-difference operator, σ_{ZWD} is the a priori standard deviation of ZWD, and it is set to 2 cm in this study based on the accuracy of GFS ZWD product (Lasota et al. 2020).

UDUC PPP-RTK user model

In the UDUC PPP-RTK user model, the rank deficiency problem is similar to that of the network model. The network model transmits estimated parameters, including satellite clock error $d\tilde{t}^s$, satellite phase biases $\tilde{\delta}_j^s$, and atmospheric products to users as state-space representation (SSR) using broadcast communication links. Satellite

clock error $d\tilde{t}^s$ and satellite phase biases $\tilde{\delta}_j^s$ are used to directly correct the satellite clock error and satellite phase biases, respectively, in the user model. Ionospheric delay $E\left[l_u^s\right]$ and ZWD $E\left[\tau_u\right]$ products are interpolation results from the network stations, and they constrain the user model with a priori information. Considering that the user model estimates the difference ZWD between the datum reference station and the user station, and that users usually cannot obtain information of the datum reference station in practical applications, GFS ZWD constraints are not used in the user model. Finally, the full-rank UDUC PPP-RTK user model is given as follows:

$$E\left[p_{u,j}^s + d\tilde{t}^s\right] = g_u^s \Delta x_u + m_u^s \tilde{\tau}_u + d\tilde{t}_u + \mu_j \tilde{l}_u^s + \mu_j \tilde{d}_{u,GF}$$

$$E\left[\phi_{u,j}^s + d\tilde{t}^s + \tilde{\delta}_j^s\right] = g_u^s \Delta x_u + m_u^s \tilde{\tau}_u + d\tilde{t}_u - \mu_j \tilde{l}_u^s + \tilde{\delta}_{u,j} + \lambda_j \tilde{z}_{u,j}^s$$

$$E\left[l_u^s\right] = \tilde{l}_u^s$$

$$E\left[\tau_u\right] = \tilde{\tau}_u$$

$$\qquad (12)$$

In the user model, the estimable unknown parameters are the same as those in the network model as shown in Table 1, except the user positioning parameters Δx_u. The parameter process noise settings and stochastic model scheme are consistent with the network model. The LAMBDA (Least-squares AMBiguity Decorrelation Adjustment) method has been used for integer ambiguity resolution (Teunissen 1998).

Results and analysis

Experimental setup

Three GNSS networks from the US, Australia, and Europe regions are selected, as shown in Fig. 1a. The three GNSS networks are from different organizations: the National Geodetic Survey (NGS) of the US, Geoscience Australia (GA), and the European Reference Permanent GNSS Network (EPN). For all three networks, GPS dual-frequency code and carrier phase datasets collected over a 10-day period from March 1, 2022 (DOY: 60) to March 10, 2022 (DOY: 69) are selected with a data interval of 30 s. As shown in Fig. 1b–d, some GNSS stations are used as network stations to provide satellite clock error, satellite phase biases, and atmospheric products for the user stations, and the other GNSS stations, called user stations, are used for precise positioning test. The network provides these products to the users at each epoch with a 30-s interval, matching the user's GNSS sampling rate. This study does not consider the time delay introduced to users by network product broadcasting. For the three networks from NGS, GA, and EPN, the average

Fig. 1 **a** The global distribution of NGS, GA, and EPN networks located in the US, Australia, and Europe, respectively. **b–d** Distribution of the reference stations and user stations of NGS, GA, and EPN networks, respectively. Blue triangles for non-datum network stations, blue circle for datum stations, and red triangles for user stations
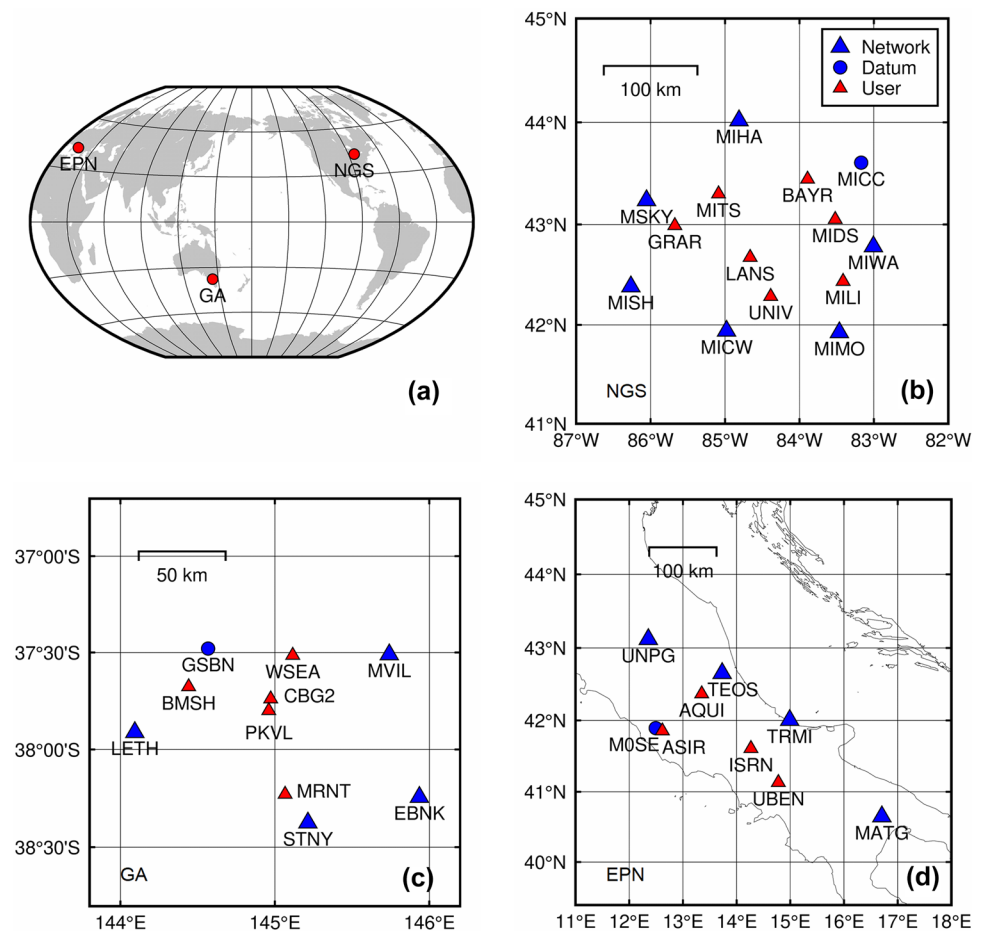

interstation distance is 115.2 km, 85.3 km, and 194.7 km, respectively. GFS global atmospheric prediction products for the 10-day period (DOY: 60–69) are downloaded from the NCEP, US, with grib2 form, from which a priori ZWD is generated for the GFS ZWD-augmented PPP-RTK (network) model (NCEP 2015). It is unnecessary to consider the time delay of GFS products, as they are forecast products that can be preloaded. A priori GFS ZWD values with 30-s intervals are obtained through linear time interpolation to match the sampling rate of GNSS observations in the network model, ensuring that constraints are applied to each epoch of the network model.

GFS products analysis

In the UDUC PPP-RTK network model, the estimated ZWD parameter is in single-difference form. The difference ZWD (dZWD) result is the difference between ZWD value at the reference stations and that of the datum reference station. Therefore, the GFS a priori ZWD values should also be formulated in the single-difference form between the reference station and the datum reference station to ensure consistency. In this study, MICC, GSBN, and M0SE serve as the

datum reference stations of the NGS, GA, and EPN networks, respectively. With that, 10-day GFS a priori dZWD values for all reference stations are generated for the three networks. At the same time, we estimate 10-day continuous dZWD value for all reference stations using the traditional UDUC PPP-RTK network model. In the traditional model, the functional model of Eq. (8) is employed but without the GFS ZWD constraint. Subsequently, a comparison is made between the estimated dZWD and the original GFS a priori dZWD to evaluate the reliability of the GFS products. Figure 2 compares the 10-day estimated dZWD by PPP-RTK (blue line) and GFS a priori dZWD (red line) for all reference stations in the three networks. Figure 2 shows that the dZWD estimated from PPP-RTK and the GFS a priori dZWD have a good consistency in all three networks. Pearson correlation coefficient, a statistic that quantifies the linear relationship and correlation between two variables (Akoglu 2018), is employed to measure the strength of the linear association between the two types of dZWD. The two kinds of dZWD values have high correlation coefficients (CC), as shown in Fig. 2. In general, a correlation value greater than 0.6 is regarded as a strong positive correlation (Akoglu 2018). The t-test (significant level $P < 0.05$) has

Fig. 2 Comparison between estimated dZWD by UDUC PPP-RTK (blue) and GFS a priori dZWD (red) for all non-datum reference stations in NGS (**a**), GA (**b**), and EPN (**c**) networks. Correlation coefficients (CC) between the two time series are shown for each reference station. Convergence process of UDUC PPP-RTK dZWD is not shown in the time series
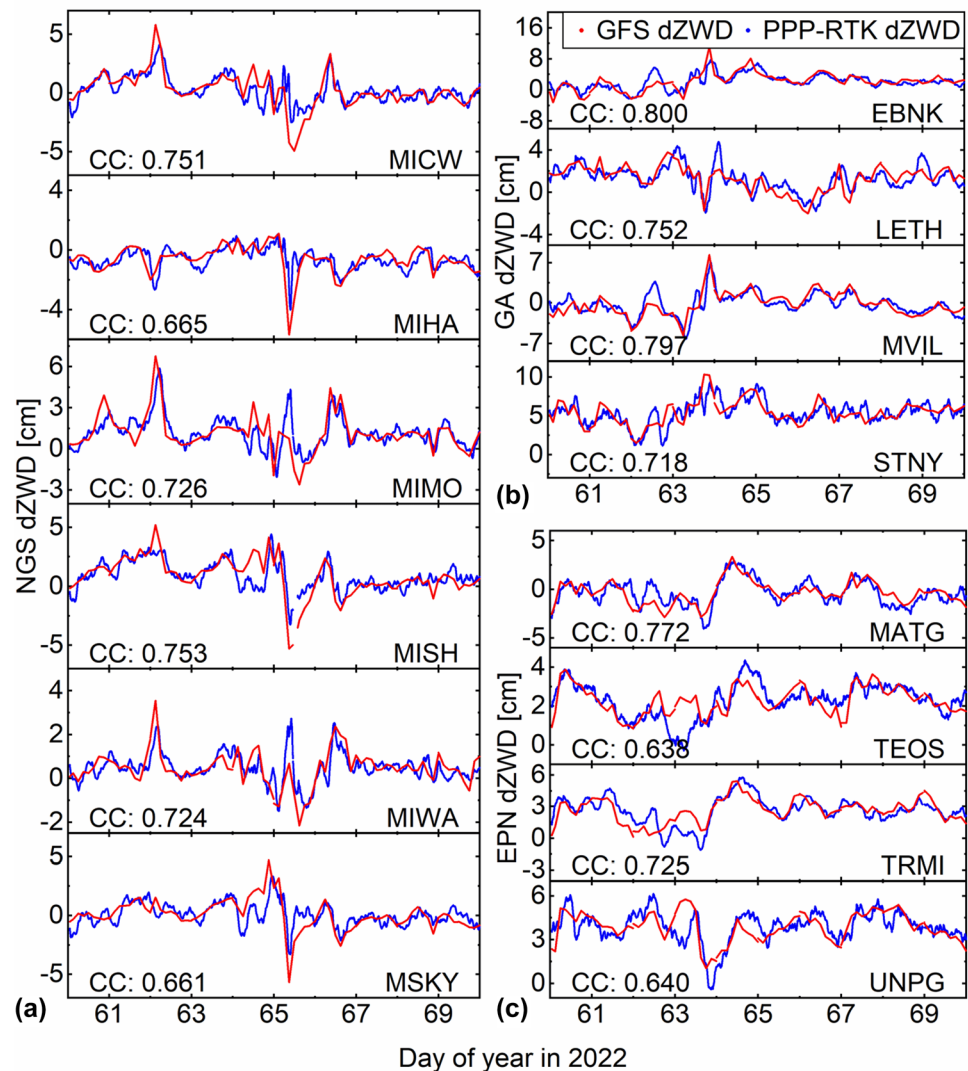
been conducted to compare the means of two groups and ascertain whether the observed differences between them are more likely to occur due to random chance (Kim 2015). Therefore, their positive correlation property indicates that GFS a priori dZWD can provide effective constraint information for the network dZWD estimate.

Network ZWD product generation

For a more effective comparison, the traditional PPP-RTK network model, which utilizes Eq. (8) but excludes the GFS ZWD constraint, also generates ZWD products using the estimated ZWD parameters. These ZWD products generated by the traditional PPP-RTK network model are then provided to user stations using the same interpolation method as the GFS ZWD-augmented PPP-RTK model. To be specific, in both traditional (without constraint) and GFS ZWD-augmented (with a priori GFS ZWD constraint) PPP-RTK

network models, dZWD parameters of all non-datum reference stations are estimated. After obtaining the dZWDs of all the non-datum reference stations, the inverse distance weight interpolation method is used in both traditional and GFS ZWD-augmented PPP-RTK to calculate the dZWD at user stations based on the precise position of reference stations and approximate position of user stations (Lu and Wong 2008). Besides the a priori GFS ZWD constraint integrated into the GFS-augmented PPP-RTK network model, both the traditional PPP-RTK model and the GFS-augmented PPP-RTK model employ identical parameter processing and filtering strategy. Figure 3 shows the comparison of ZWD products generated from the traditional and the GFS ZWD-augmented PPP-RTK network model and the time series of the difference values between these two kinds of dZWD. Both methods restart the Kalman filter of the network model at 0:00 every day, and the black dashed line indicates the restart time. As shown in Fig. 3, in the initial
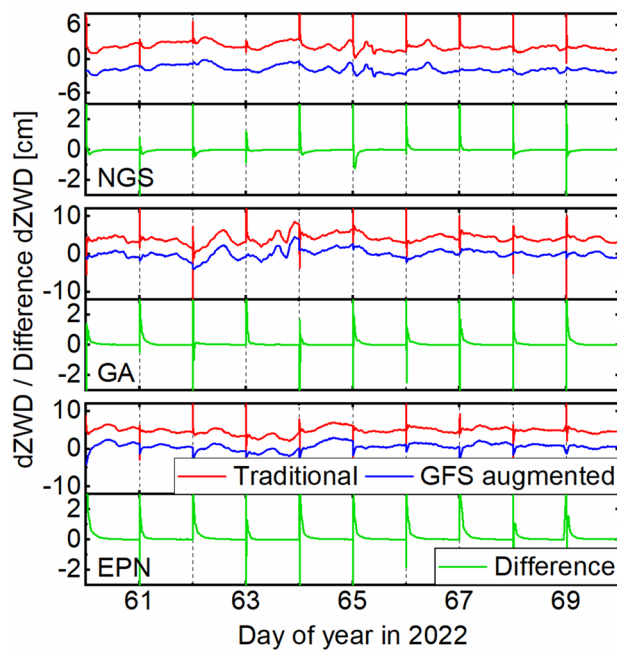
Fig. 3 Comparison of dZWD estimated at three user stations using traditional PPP-RTK network model (red) and GFS ZWD-augmented PPP-RTK network model (blue). Their difference is shown in the sub-plot below (green). The three user stations BAYR, CBG2, and ASIR are from the NGS, GA, and EPN networks, respectively. It should be noted that the offset values of 2 cm and − 2 cm have been added to the dZWD solution of the traditional PPP-RTK network model (red) and GFS-augmented PPP-RTK (blue), respectively, for better visualization purpose

Fig. 4 Comparison of 10-day average convergence time between traditional (orange) and GFS ZWD-augmented PPP-RTK (green) products at all the user stations in the NGS, GA, and EPN networks. The average convergence time is calculated by averaging the convergence time values from every Kalman filter initialization for each user station

User station convergence time and positioning performance

stage of Kalman filtering, the traditional PPP-RTK network model fails to provide precise ZWD products, and it needs time to converge. The GFS ZWD-augmented PPP-RTK network model (blue line) produces more accurate dZWD result in the initial filtering stage and barely needs a convergence time. The difference results (green line) can clearly show this. It is noticed that after Kalman filter convergence, the dZWD estimation tends to converge for both methods and their difference approaches to zero. This implies that the GFS a priori ZWD product is very effective in the initial stage of the Kalman filter, but its contribution will decrease with time when the filter has enough GNSS observations to estimate the accurate ZWD parameter (filter convergence). Therefore, when the network filter needs to be restarted for reasons such as offline datum reference stations, the GFS a priori ZWD data can help user stations obtain a converged PPP-RTK solution more quickly than traditional one.

To evaluate the positioning performance of the GFS ZWD-augmented PPP-RTK network model, we analyzed the 10-day positioning results of 16 user stations from the three networks and compared them with the positioning results based on traditional PPP-RTK network products. For a fair comparison, the user positioning strategy used in traditional PPP-RTK is identical to that of GFS ZWD-augmented PPP-RTK. In the user model of traditional PPP-RTK, the STD of ZWD pseudo-observation generated from the network model is also set as 2 cm, the same as the user model of the GFS-augmented PPP-RTK.

In this test, the network model Kalman filter restarts at 00:00 every day to evaluate the contribution of GFS a priori ZWD data on convergence. For user stations, convergence time is an important index of positioning performance. In this study, convergence time is defined as the minimum observation time span required to achieve positioning errors

Fig. 5 User positioning time series of traditional (left) and GFS-augmented (right) PPP-RTK models for the dataset collected at BAYR from the NGS network on DOY 60. Both ambiguity float solution (red) and ambiguity-fixed solution (blue) are shown. The time scale in the first 2 h is intentionally enlarged to illustrate the convergence time
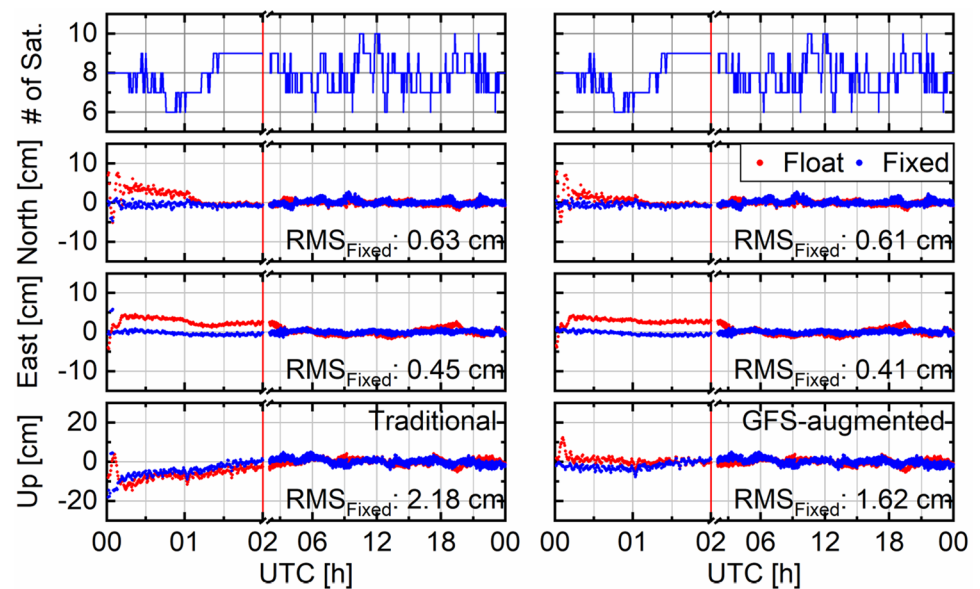
below 10 cm for at least 60 min. At every user station, the convergence time is calculated each day, and average convergence time over the 10-day period is obtained. Figure 4 shows the comparison of convergence time of employing GFS-augmented and traditional PPP-RTK products. As shown in Fig. 4, GFS-augmented network data can significantly shorten user station positioning convergence time for all the user stations in the three networks. This is due to the rapid convergence of tropospheric parameter estimated by the network model after the introduction of GFS a priori information. For all the 16 user stations, the average convergence time is reduced by 46% from 10.0 to 5.4 min. To show the advantage of GFS-augmented clearly, the positioning time series at DOY 60 of BAYR station based on GFS-augmented and traditional network data are compared and shown in Fig. 5. We are shown from Fig. 5 that the contribution of GFS a priori ZWD is mostly effective in the up direction. This can be explained as GFS a priori ZWD mostly improves the accuracy of ZWD products in the PPP-RTK network model, and the positioning performance in the up direction is the most sensitive to the ZWD accuracy. We can also note that as the filtering progresses, the positioning performance of GFS-augmented PPP-RTK gradually becomes similar to that of traditional PPP-RTK. This is because after a certain period of time, enough GNSS observations have been collected, and the traditional PPP-RTK network model can also provide accurate ZWD data for the user stations.

Short-term precision is defined as the positioning precision of short-term time intervals in the initial stage of Kalman filtering (Lu et al. 2017). As the convergence time is reduced after applying the GFS ZWD data, the short-term precision is also expected to be improved. In this study, we calculate the short-term RMS errors in a 20-min time interval for the first 100 min of the whole Kalman filter process at every user station. It is noticed that the Kalman filter in the network model restarts on a daily basis, and the final result for short-term RMS is calculated by averaging the 10-day results. We randomly select three user stations (BAYR, CBG2, and ASIR) from the three different regional networks and compare their short-term precision using GFS-augmented and traditional PPP-RTK network ZWD data. These results are shown in Fig. 6. At the three user stations, the accuracy improvement resulting from the GFS a priori ZWD information is obvious in the initial stage of the Kalman filter. However, when time progresses, the accuracy advantage of GFS-augmented method gradually decays, especially in horizontal components, which is consistent with the findings in the single-station positioning results shown in Fig. 5.

We also calculated the 10-day positioning 3D-RMS errors of the user stations. These values are calculated using the positioning results obtained from the entire filter processing. The PPP-RTK network Kalman filter is restarted at 00:00 on a daily basis. To calculate the positioning RMS errors, the long-term static PPP positioning results provided by the NGS, GA, and EPN are used as the reference coordinates of the stations. Figure 7 shows the positioning 3D-RMS errors of all user stations in this research. At the same time, Table 2 shows the 3D-RMS errors of both traditional and GFS ZWD-augmented PPP-RTK network products and the percentage of the improvement of GFS-augmented products. As shown in Fig. 7 and Table 2, for all the user stations, the positioning accuracy of GFS-augmented method is better than that of the traditional method. Taking the station MIDS in the NGS network as an example, the GFS-augmented method reduces its 3D-RMS positioning error by 9.56%,
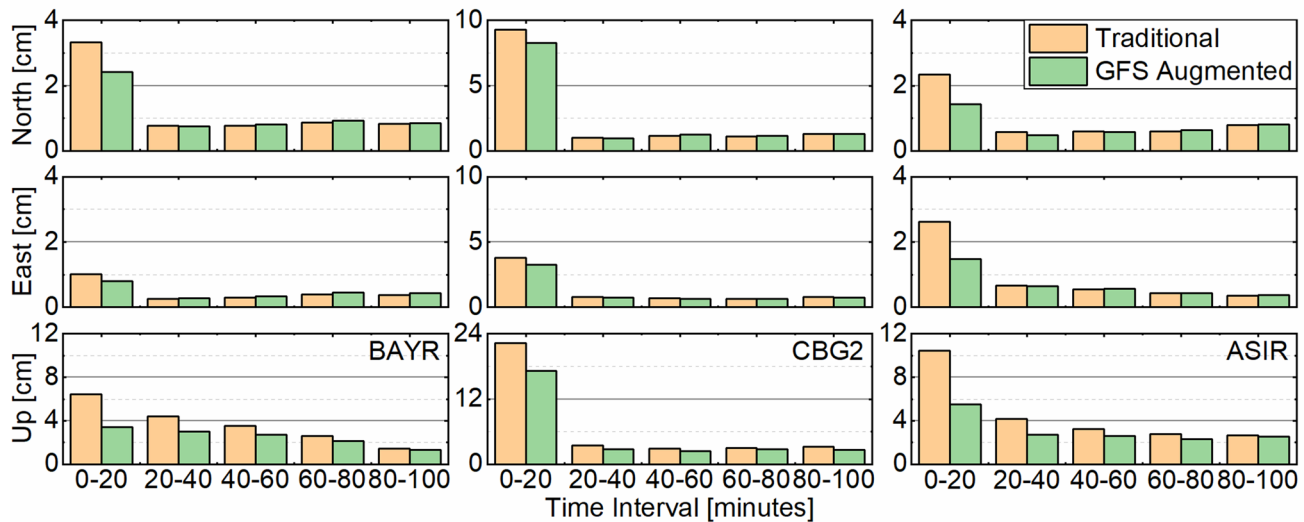
Fig. 6 Comparison of average RMS values of short-term user positioning between traditional (orange) and GFS ZWD-augmented (green) PPP-RTK. Three user stations BAYR, CBG2, and ASIR from NGS, GA, and EPN networks, respectively, are selected. Twenty-min time interval is used. The average short-term RMS is calculated by averaging the short-term RMS errors from every Kalman filter initialization for BAYR, CBG2, and ASIR
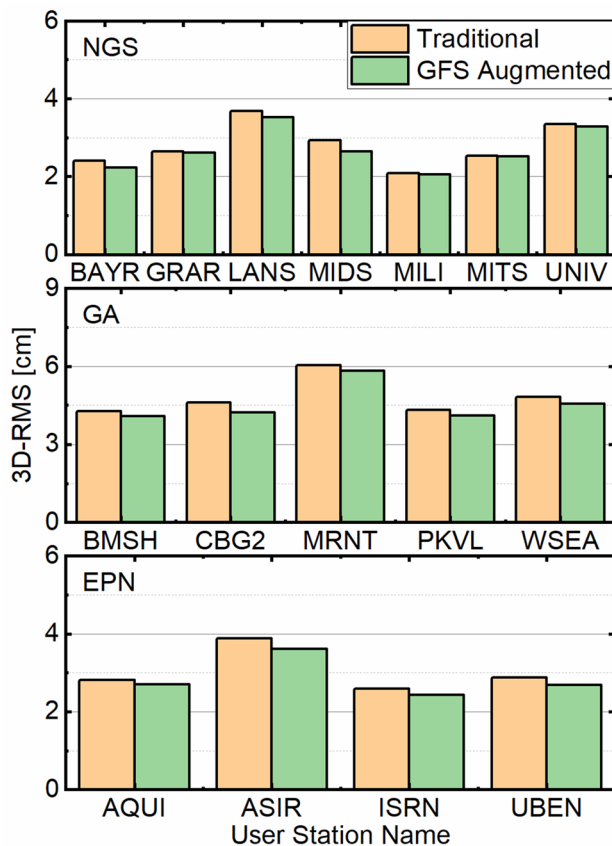
from 2.93 to 2.65 cm. For all the 16 user stations, the average 3D-RMS error is reduced by 5.7% from 3.5 to 3.3 cm.

The contribution of GFS ZWD-augmented PPP-RTK to ambiguity resolution

This section uses a partial ambiguity-fixed technique based on the LAMBDA method to obtain the ambiguity-fixed solutions (Parkins 2011). The successful fixing of integer ambiguities is based on the two criteria: (1) Ambiguity resolution passes the ratio test, with a ratio threshold of two, and (2) the final successfully fixed ambiguities must account for over 60% of the total ambiguities in the original ambiguity list for the current epoch (Zhang et al. 2022). The ambiguity fixing rate is the percentage of epochs with successful ambiguity fixing over the total epochs of all days, and the epochs within the convergence period have been included too. The ambiguity fixing rates of both the traditional and GFS ZWD-augmented PPP-RTK methods are calculated for all the user stations. Table 3 shows the ambiguity fixing rate and the improvements of GFS-augmented method. Results show that the GFS a priori ZWD information used in the PPP-RTK network model only slightly improves the ambiguity fixing rate at most user stations. This is because the advantages of GFS-augmented PPP-RTK are mostly evident during the short-term convergence process after filter starts. When considering the entire solution process, the improvements appear not so significant. In addition, the LAMBDA algorithm is robust and resistant to biases in ambiguities (Li et al. 2014). This implies that even if there is a bias in the ZWD information used by the user stations, the ambiguities can

Fig. 7 Comparison of 10-day positioning 3D-RMS errors between traditional (orange) and GFS ZWD-augmented PPP-RTK (green) for all the user stations from the three networks

Table 2 Comparison of positioning accuracy between the traditional and the GFS ZWD-augmented PPP-RTK models and the percentage of improvement of the GFS ZWD-augmented PPP-RTK model over the traditional one

GNSS network	Station	Traditional model 3D-RMS (cm)	GFS-augmented model 3D-RMS (cm)	RMS reduction of the GFS model (%)
NGS	BAYR	2.40	2.23	7.08
	GRAR	2.64	2.62	0.76
	LANS	3.68	3.52	4.35
	MIDS	2.93	2.65	9.56
	MILI	2.08	2.06	0.96
	MITS	2.53	2.53	0.00
	UNIV	3.35	3.29	1.79
GA	BMSH	4.28	4.08	4.67
	CBG2	4.61	4.21	8.68
	MENT	6.03	5.83	3.32
	PKVL	4.32	4.09	5.32
	WSEA	4.82	4.55	5.60
EPN	AQUI	2.81	2.69	4.27
	ASIR	3.88	3.62	6.70
	ISRN	2.60	2.43	6.54
	UBEN	2.88	2.69	6.60

Table 3 Comparison of the ambiguity fixing rates of traditional PPP-RTK and the GFS ZWD-augmented PPP-RTK models at each user station of the three networks

Organization	Station	Traditional model ambiguity fixing rate (%)	GFS-augmented model ambiguity fixing rate (%)	Improvements (%)
NGS	BAYR	96.98	96.86	− 0.12
	GRAR	81.30	81.50	0.25
	LANS	57.63	57.84	0.36
	MIDS	92.99	93.10	0.12
	MILI	96.46	96.13	− 0.34
	MITS	77.50	77.72	0.28
	UNIV	86.39	88.53	2.42
GA	BMSH	93.68	94.11	0.45
	CBG2	96.19	96.60	0.42
	MENT	81.12	81.86	0.90
	PKVL	88.20	87.98	− 0.25
	WSEA	91.39	91.36	− 0.03
EPN	AQUI	77.71	77.67	− 0.05
	ASIR	78.72	79.14	0.53
	ISRN	96.78	96.83	0.05
	UBEN	94.18	94.26	0.08

still be successfully fixed, thereby minimizing the impact of GFS ZWD information. We can also notice from Table 3 that for a small number of user stations, GFS ZWD even has a negative impact on the ambiguity fixing rate. This might be because the GFS ZWD is less accurate than the estimated ZWD, leading to a decrease in ambiguity fixing rate.

We also calculate the TTFF for all the user stations by averaging their TTFF values from every Kalman filter initialization. There are ten initializations in total for each user station. The TTFF is defined as the minimum observation time required to achieve ambiguity-fixed success. Figure 8 shows the TTFF comparison results from both traditional PPP-RTK and the GFS ZWD-augmented PPP-RTK models. The results indicate that GFS-augmented information can greatly reduce the TTFF for most stations. The average TTFF value is reduced by 35.8% for all the user stations from 6.7 min to 4.3 min. It further verifies the effectiveness of using GFS a priori ZWD products in the initial stage of the Kalman filter.
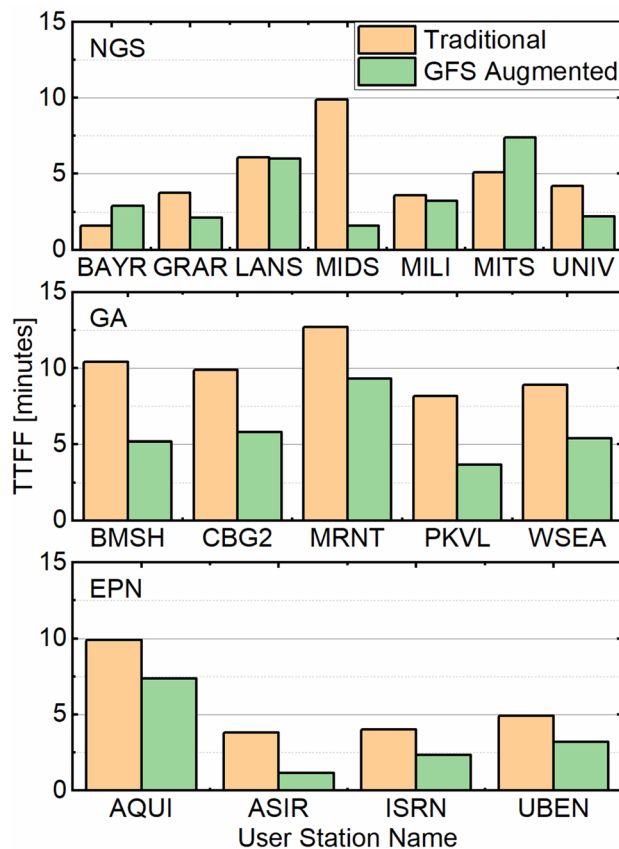
Fig. 8 Comparison of average TTFF between traditional (orange) and GFS ZWD-augmented PPP-RTK (green) at each user station of the three networks. The average TTFF is calculated by averaging the TTFF values from every Kalman filter initialization for each user station

Conclusion

In this work, the GFS-augmented UDUC PPP-RTK model has been developed. The GFS product is employed to generate a priori ZWD values, which are then used to constrain the ZWD parameter in the PPP-RTK network model to provide ZWD data for the PPP-RTK user stations. To test the performance of GFS product and its compatibility with the PPP-RTK technique, 10-day GNSS data from three GNSS networks in the US, Australia, and Europe are analyzed.

The consistency between the GFS ZWD product and ZWD data estimated by UDUC PPP-RTK network is systematically analyzed. The results show that the correlation coefficient between the ZWD generated from the GFS products and the ZWD estimated from PPP-RTK network model can achieve a value between 0.64 and 0.80. This verifies the compatibility and effectiveness of the GFS ZWD product for the UDUC PPP-RTK model.

The GFS ZWD-augmented PPP-RTK model is used to conduct positioning test for 16 user stations from the three networks. The results show that with the GFS ZWD a priori information in the network model, the positioning performance of the user stations improves significantly in terms of convergence time, positioning accuracy, and the TTFF values. The GFS ZWD-augmented PPP-RTK can also slightly improve the ambiguity fixing rate. Analyzing all the 16 user stations over a 10-day period, GFS ZWD-augmented PPP-RTK reduces the average convergence time by 46% from 10.0 to 5.4 min, 3D-RMS error by 5.7% from 3.5 to 3.3 cm, and the time to first fix value by 35.8% from 6.7 to 4.3 min. This clearly shows the advantage of GFS-augmented PPP-RTK for user positioning, especially in the initial stage of the Kalman filter. As the filtering progresses, the advantage of a priori GFS ZWD information gradually decays, and GFS-augmented PPP-RTK shows a positioning performance similar to traditional PPP-RTK.

Declarations

References

Accadia C, Mariani S, Casaioli M, Lavagnini A, Speranza A (2003) Sensitivity of precipitation forecast skill scores to bilinear interpolation and a simple nearest-neighbor average method on high-resolution verification grids. Weather Forecast 18:918–932

Akoglu H (2018) User's guide to correlation coefficients. Turk J Emerg Med 18:91–93

Bevis M, Businger S, Chiswell S, Herring T, Anthes R, Rocken C, Ware R (1994) GPS meteorology-mapping zenith wet delays onto precipitable water. J Appl Meteorol 33:379–386

Böhm J, Möller G, Schindelegger M, Pain G, Weber R (2015) Development of an improved empirical model for slant delays in the troposphere (GPT2w). GPS Solut 19:433–441

Cui B, Wang J, Li P, Ge M, Schuh H (2022) Modeling wide-area tropospheric delay corrections for fast PPP ambiguity resolution. GPS Solut 26:56

Deng C, Tang W, Liu J, Shi C (2014) Reliable single-epoch ambiguity resolution for short baselines using combined GPS/BeiDou system. GPS Solut 18:375–386

Eueler H, Goad C (1991) On optimal filtering of GPS dual frequency observations without using orbit information. Bull Geodesique 65(2):130–143

Gao R, Liu Z, Odolinski R, Jing Q, Zhang J, Zhang H, Zhang B (2023) Hong Kong–Zhuhai–Macao bridge deformation monitoring using PPP-RTK with multipath correction method. GPS Solut 27(195):1–15

Gurturk M, Soycan M (2021) Accuracy assessment of kinematic PPP versus PPK for GNSS flights data processing. Surv Rev 2:1–9

Han J, Pan H (2011) Revision of convection and vertical diffusion schemes in the NCEP global forecast system. Weather Forecast 26:520–533

Hou P, Zhang B (2023) Decentralized GNSS PPP-RTK. J Geodesy 97:72

Kim T (2015) T test as a parametric statistic. Korean J Anesthesiol 68:540–546

Kleijer F (2004) Troposphere modeling and filtering for precise GPS leveling. 99–104

Kouba J (2008) Implementation and testing of the gridded Vienna mapping function 1 (VMF1). J Geodesy 82:193–205

Lasota E, Rohm W, Guerova G, Liu C (2020) A comparison between ray-traced GFS/WRF/ERA and GNSS slant path delays in tropical cyclone meranti. IEEE Trans Geosci Remote Sens 58:421–435

Leandro R, Langley R, Santos M (2008) UNB3m_pack: a neutral atmosphere delay package for radiometric space techniques. GPS Solut 12:65–70

Li B, Verhagen S, Teunissen P (2014) Robustness of GNSS integer ambiguity resolution in the presence of atmospheric biases. GPS Solut 18:283–296

Li P, Cui B, Hu J, Liu X, Zhang X, Ge M, Schuh H (2022) PPP-RTK considering the ionosphere uncertainty with cross-validation. Satellite Navig 3:10

Lu G, Wong D (2008) An adaptive inverse-distance weighting spatial interpolation technique. Comput Geosci 34:1044–1055

Lu C, Li X, Zus F, Heinkelmann R, Dick G, Ge M, Wickert J, Schuh H (2017) Improving BeiDou real-time precise point positioning with numerical weather models. J Geodesy 91:1019–1029

National Centers for Environmental Prediction. (2015) NCEP GFS 0.25 degree global forecast grids historical archive. In: Research data archive at the national center for atmospheric research, Computational and Information Systems Laboratory, Boulder, CO

Odolinski R, Teunissen P, Odijk D (2015) Combined GPS plus BDS for short to long baseline RTK positioning. Meas Sci Technol 26(4):1–16

Odolinski R, Teunissen P (2017) Low-cost, high-precision, single-frequency GPS-BDS RTK positioning. GPS Solut 21(3):1315–1330

Parkins A (2011) Increasing GNSS RTK availability with a new single-epoch batch partial ambiguity resolution algorithm. GPS Solut 15:391–402

Powers J et al (2017) The weather research and forecasting model: overview, system efforts, and future directions. Bull Am Meteor Soc 98:1717–1737

Schaffrin B, Bock Y (1988) A unified scheme for processing GPS dual-band phase observations. Bull Geodesique 62(2):142–160

Teunissen P (1985) Zero order design: generalized inverses, adjustment, the datum problem and S-transformations. In: Grafarend EW, Sansò F (eds) Optimization and design of geodetic networks. Springer, Berlin, pp 11–55

Teunissen P (1998) Success probability of integer GPS ambiguity rounding and bootstrapping. J Geodesy 72(10):606–612

Teunissen P, Odolinski R, Odijk D (2014) Instantaneous BeiDou plus GPS RTK positioning with high cut-off elevation angles. J Geodesy 88(4):335–350

Teunissen P, Khodabandeh A (2015) Review and principles of PPP-RTK methods. J Geodesy 89:217–240

Theodoro L, Lima Rodrigues T, de Oliveira Jr P, Vestena K (2022) Assessment of tropospheric modeling on PPP-AR performances under brazilian atmospheric condition. Boletim de Ciencias Geodesicas 28

Wang J, Liu Z (2019) Improving GNSS PPP accuracy through WVR PWV augmentation. J Geodesy 93:1685–1705

Wilgan K, Hadas T, Hordyniec P, Bosy J (2017) Real-time precise point positioning augmented with high-resolution numerical weather prediction model. GPS Solut 21:1341–1353

Yin X, Chai H, El-Mowafy A, Zhang Y, Zhang Y, Du Z (2022) Modeling and assessment of atmospheric delay for GPS/Galileo/BDS PPP-RTK in regional-scale. Measurement 194:111043

Yu C, Li Z, Penna N (2018) Interferometric synthetic aperture radar atmospheric correction using a GPS-based iterative tropospheric decomposition model. Remote Sens Environ 204:109–121

Zhang B, Chen Y, Yuan Y (2019) PPP-RTK based on undifferenced and uncombined observations: theoretical and practical aspects. J Geodesy 93(7):1011–1024

Zhang B, Hou P, Odolinski R (2022) PPP-RTK: from common-view to all-in-view GNSS networks. J Geodesy 96(102):1–20

Rui Gao is a Ph.D. candidate at the Innovation Academy for Precision Measurement Science and Technology, CAS. His current research focuses on high-precision kinematic GNSS positioning models, algorithms, related applications, and software development.

ZhiZho Liu is a Professor at the Department of Land Surveying and Geo-Informatics, Hong Kong Polytechnic University, Hong Kong. His research interests include new algorithm development for precise GNSS positioning and navigation, GNSS precise point positioning, ionosphere and troposphere observation and modeling, and GNSS meteorology.

Baocheng Zhang is a Professor at the Innovation Academy for Precision Measurement Science and Technology, CAS. His research focuses on modeling multiple global navigation satellite systems for integer ambiguity resolution-enabled precise point positioning (PPP-RTK) applications.

Robert Odolinski is currently a Senior Lecturer at the School of Surveying, University of Otago, and a 'Visiting Researcher' at Google. He is a member of the International Association of Geodesy (IAG) ICCT Joint Study Group 'Multi-GNSS Theory and Algorithms,' a co-chair of the IAG working groups on 'Reliability of low-cost & Android GNSS in navigation and geosciences' and 'Ambiguity resolution for low-cost GNSS receiver positioning,' respectively.